A Study of the Weld Heat-Affected Zone Toughness of 9% Nickel Steel

Although thermal cycling reduces cryogenic impact toughness and upper shelf energy, ASTM specifications are still exceeded

BY E. F. NIPPES AND J. P. BALAGUER

ABSTRACT. The weld heat-affected zone toughness of 9% nickel steel weldments at cryogenic temperatures was investigated. The material was thermally treated, using a Gleeble, to produce synthetic weld heat-affected zones. Toughness of this steel, subjected to three different thermal cycles, was measured using the Charpy V-notch impact test. It was found that the material subjected to high peak-temperature thermal cycles still met the ASTM toughness requirements for this steel at liquid nitrogen temperatures. The upper shelf energy for this steel was lowest for an intermediate thermal cycle of 1000°C (1832°F) peak temperature.

A fractographic analysis of the material was conducted. Charpy V-notch specimens fractured at liquid nitrogen temperatures were examined in the scanning electron microscope. Material representative of the coarse-grained region of the heat-affected zone failed by a partially low-energy mode at cryogenic temperatures.

The retained austenite content of this material, under varying conditions of thermal treatments, was determined using standard x-ray diffraction techniques. It was found that upper shelf toughness increased as the amount of retained austenite increased, while toughness at liquid nitrogen temperatures was related to combined effects of prior austenite grain size and retained austenite content. Retained austenite was also measured using the Magne-Gage, modified for the measurement of austenite in a ferritic matrix, and these data were correlated with the x-ray diffraction results.

Introduction

Increases in demand for natural gas have made it necessary to construct storage facilities for liquefied natural gas. Because liquid natural gas (LNG) is stored at, or below, the −162°C (−260°F) boiling temperature, the vessel must be constructed from a material which possesses high strength and suitable fracture toughness at cryogenic temperatures.

Nine percent nickel steels were first produced in the United States in the early 1940's. More recently, Japanese steel companies have also begun to produce large tonnages of 9% nickel steel. The alloying addition of approximately nine percent nickel and the subsequent heat treatment are primarily responsible for the relatively high strength and excellent fracture toughness exhibited by this steel. The superb low-temperature properties of 9% nickel steel make it a good material candidate for liquid natural gas storage tanks.

Almost all the 9% nickel steel produced in the United States is intended for the fabrication of welded pressure vessels. It is well known that welding can seriously alter the metallurgical properties of the material immediately adjacent to the weld joint. Therefore, the effect of weld heat-affected zones (HAZ) on the cryogenic fracture toughness of 9% nickel steel LNG storage tanks must be properly evaluated.

Previously, the weld heat-affected zone properties of a wide variety of steels and nonferrous metals have been evaluated utilizing weld simulation devices, Charpy V-notch impact testing, and metallographic investigation. The object of the present investigation will be to evaluate the effect of weld thermal cycles on the impact absorption energy of the weld HAZ of 9% nickel steel at cryogenic temperatures.

Metallurgical Characteristics

The fundamental mechanical properties of 9% nickel steel must meet the minimum requirements of ASTM 353 or ASTM 553 Type I specifications, as shown in Table 1. ASTM 353 and 533 Type I specify double-normalize-and-temper (NNT) and quench-and-temper (QT) heat treatments, respectively. These specifications require measurement of impact absorption energy at liquid nitrogen temperatures, −196°C (−320°F). However, at the LNG storage temperature of −162°C (−260°F), these steels, in the wrought condition, safely exceed the ASTM specifications described in Table 1.

The excellent low-temperature toughness of this steel results from the alloying addition of approximately nine percent nickel. The nickel acts to suppress the formation of ferrite/pearlite high-temperature transformation products; thus, a microstructure is produced which is higher in strength and notch toughness. It is generally recognized that the superior fracture toughness of 9% nickel steel at cryogenic temperatures is due to the presence of stable retained austenite (Refs. 1–5). The addition of nickel lowers the martensite finish temperature such that unstable austenite remains after cooling from the austenitization temperature to room temperature.

Previous investigations (Refs. 3, 5, 6) have shown that if tempering is performed in the two-phase $\alpha + \gamma$ region above the lower critical temperature, *i.e.*, above approximately 580°C (1076°F), the high nickel content stabilizes the austenite, and the final product contains 5 to 10 volume percent (v-%) "retained" austenite. This second phase increases low-temperature toughness primarily by scavenging interstitials, and this scavenging

Based on a paper presented at the 66th AWS Annual Meeting, held April 28 to May 3, 1985, in Las Vegas, Nev.

E. F. NIPPES is Professor of Metallurgical Engineering, and J. P. BALAGUER is Research Fellow, Department of Materials Engineering, Rensselaer Polytechnic Institute, Troy, N. Y.

Table 1—ASTM 553-I Specifications for 9% Nickel Steels

	C	Mn	P	S	Si	Ni
Composition (v-%)	0.13 max.	0.90 max.	0.035 max.	0.040 max.	0.15–0.40	8.5–9.5

Tensile Requirements (20°C)	Tensile Strength MPa (ksi)	Yield Strength, min. MPa (ksi)	Elongation in 50 mm, min.%
	690–825 (100–120)	585 (85)	20.0

Impact Absorption Energy (Charpy V-Notch) at −196°C	Longitudinal, min. J (ft-lb)	Transverse, min. J (ft-lb)
	34 (25)	27 (20)

Heat Treatment	Austenitizing Temperature °C (°F)	Tempering Temperature °C (°F)
	800–925 (1475–1700)	565–635 (1050–1175)

Table 2—Chemical Analysis of Base Plate Used in This Investigation (Ref. 19)

Element	C	Mn	P	S	Si	Ni	Fe
v-%	0.05	0.71	0.018	0.019	0.41	8.90	bal.

Table 3—Mechanical Properties of Base Plate Used in This Investigation (Ref. 19)

Tensile Strength MPa (ksi)	Yield Strength MPa (ksi)	Elongation %	Test Temperature °C (°F)
742 (107.5)	695 (100.7)	26.4	20 (68)
1005 (145.7)	905.5 (131.2)	27.1	−162 (−260)
1118.5 (162.1)	984 (142.6)	29.3	−196 (−321)

Tensile properties – longitudinal plate orientation.
Values reported represent average of two tests.

action prevents the formation of embrittling carbides and nitrides. The resulting decrease in yield strength and increase in work-hardening ability increases fracture toughness. During tempering, the austenite also gathers uncombined carbon, which is thought to initiate cleavage cracks in martensite (Ref. 2). Kim (Ref. 6) and Schwartz (Ref. 7) have proposed that additional mechanisms, including the blunting of cleavage crack tips upon entering regions of retained austenite, may operate to a lesser degree than the scavenging effect. However, recent work by Kim and Morris (Ref. 8) on a 5.5% nickel steel suggests that the crack blunting hypothesis is unlikely. They propose that the reduced effective grain size of a composite microstructure is responsible for the high observed toughness at cryogenic temperatures.

Simulation and Analysis of Weld Heat-Affected Zones

Welding can seriously alter the metallurgical properties and the stress state of the material immediately adjacent to the weld joint. The intense heat of a welding arc can subject the surrounding material to severe thermal cycles. The thermal cycles always alter, to some extent, the metallurgical structure of the base material near the weld. This region, referred to as the weld heat-affected zone (HAZ), has been studied extensively by Nippes (Ref. 9) and others. The methodology of simulating the weld HAZ used in this study, *i.e.,* reproduction of measured weld thermal cycles in a small specimen using the Gleeble machine, is an intrinsic part of the welding literature. A detailed discussion of these techniques can be found elsewhere (Refs. 9–11).

The effect of weld heat-affected zones on the cryogenic fracture toughness of 9% nickel steel LNG storage tanks has been the subject of recent study. The fracture toughness of this material has been evaluated using both traditional testing methods, such as Charpy V-notch (CVN) and crack-opening displacement (COD) tests, and more advanced methods, such as J-integral and R-curve techniques. The variety of testing methods and the inconsistencies of weld HAZ structures have resulted in contradicting data on the fracture toughness of the HAZ in 9% nickel steel welded joints (Refs. 12–18).

Dhooge, *et al.* (Ref. 16), have suggested that the thermal cycles to which the HAZ is subjected can reduce the impact energy of this region by almost fifty percent. Similarly, Syn, *et al.* (Ref. 5), have found that the retained austenite content of 9% nickel steel is reduced to immeasurable levels by elevated temperature treatments. Dhooge, *et al.* (Ref. 16), have also found that a postweld heat treatment at 600°C (1112°F), followed by rapid air cooling or water quenching, would increase the toughness of the weld HAZ.

Materials and Procedure

Characterization of Base Material

The base material used in this investigation is a quench-and-tempered 9% nickel steel. The material was obtained in the form of 12-mm (0.47-in.) thick plate. The chemical analysis of the plate, shown in Table 2, meets the compositional requirements of ASTM 553-I. The fundamental mechanical properties of this alloy are shown in Table 3.

The impact absorption energy of the base material as a function of temperature, measured using the Charpy V-notch impact test, is shown in Fig. 1. It is difficult to determine the ductile-to-brittle transition temperature of this material from these data because the lower energy shelf is not clearly defined. If it is assumed that the lower energy shelf begins at −196°C, the transition temperature, defined as one-half the sum of the upper and lower shelf energies, appears to be approximately −120°C (−184°F). The average impact absorption energy of this material at −196°C was about 110 J (86 ft-lb), considerably higher than the 34 J

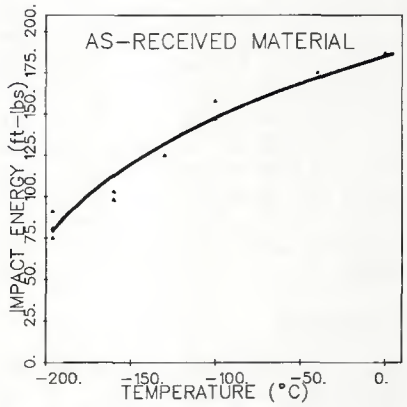

Fig. 1—Impact energy vs. temperature for material in the as-received condition

(25 ft-lb) minimum specified by ASTM 553-I. The average impact absorption energy at the LNG service temperature (−162°C) was about 135 J (101 ft-lb).

The macrohardness and microhardness of the as-received material were HRC 20 and HV 259, respectively. Grain size estimates of the as-received and heat-treated material were prepared in accordance with ASTM E112, using the intercept method.

Simulation of Weld Heat-Affected Zones

Oversized Charpy V-notch specimen blanks were machined from the base material plate and thermally cycled in a Gleeble to produce synthetic weld heat-affected zones. The oversized dimensions allowed removal of surface oxide resulting from thermal cycling by final machining prior to notching of the specimens to specified dimensions. A 0.254-mm (0.010-in.) diameter, two-wire, chromel-alumel thermocouple, percussion welded to the side of the specimen blanks, was used for temperature control in the Gleeble. The thermocouple-base metal joint was later removed during the machining of the notch in the Charpy specimen.

The specific welding thermal cycles used in this investigation were calculated utilizing the data of Nippes, Merrill, and Savage (Ref. 20) for arc welds in 12.5-mm (0.5-in.) plate. Thermal cycles for welds of 15.75 kJ/cm (40 kJ/in.) energy input and an initial plate temperature of 22°C (72°F) were calculated. Distances of 10.4, 7.9, and 7.4 mm (0.41, 0.31, and 0.29 in.) from the weld centerline were chosen to produce peak temperatures of 500°, 1000°, and 1300°C (932°, 1882°, and 2372°F), respectively.

Impact Absorption Energy Testing

Following the thermal cycling treatment, specimen blanks were machined to final dimensions of 10 × 10 × 55 mm (0.394 × 0.394 × 2.165 in.) and notched. Charpy V-notch specimen preparation procedures and impact testing were performed in accordance with ASTM E-23.

Impact absorption energy testing was performed using a Riehle Charpy V-notch testing machine. Prior to testing, the Riehle machine was calibrated with specimens provided by the United States Army Materials and Mechanics Research Center, Watertown, Massachusetts. Testing temperatures of 0°C to −162°C were obtained using a bath of 2-methylbutane cooled with liquid nitrogen. Testing temperatures of −196°C were obtained with liquid nitrogen. Specimens were maintained in a liquid bath at the test temperature for 5 min prior to impact testing. Three specimens were tested at each temperature for the 1300°C and 1000°C thermal cycles; two specimens were tested at each temperature for the 500°C thermal cycle.

Metallography

All samples in this investigation were prepared for metallographic examination using standard techniques. Samples were embedded in 31.75-mm (1.25-in.) diameter bakelite mounts and prepared by successive stages of lapping, grinding, and mechanical polishing. The following chemical etchants were used to prepare the sample for viewing under the optical microscope: Etchant A − 2% Nital; Etchant B − 2 g picric acid, 100 cc H_2O.

Measurement of Retained Austenite

X-ray diffractometry was used to determine the amount of retained austenite present in thermally cycled specimens of this steel. The method of Miller (Ref. 21), which compares the integrated peak intensities of ferritic and austenitic phases, was used.

An Aminco Model 5-660 Magne-Gage was also used to estimate the retained austenite content of specimens subjected to the various heat treatments used in this study. The Magne-Gage is normally used to measure a small amount (≃0–15 v-%) of ferrite in largely austenitic materials. However, Kotecki (Ref. 22) has shown that the Magne-Gage can be modified to measure volume percent ferrite in partially and fully ferritic steels. Ferrite and martensite, both ferromagnetic phases, and retained austenite, a non-magnetic phase, are normally present in the microstructure of 9% nickel steel. Therefore, the attractive magnetic force of the sample, measured by the Magne-Gage, should vary inversely with the volume percent of retained austenite.

In the present study, the Magne-Gage was not physically modified. A 0.25-mm (0.010-in.) thick plastic shim was placed between the specimen and the magnet during measurement. The purpose of the plastic shim was to reduce the strength of the Magne-Gage magnet. This alteration resulted in the increased sensitivity necessary to measure large amounts of ferrite. The Magne-Gage measurements were taken on three separate areas of each specimen, and the measurements were repeated ten times per area. Data were recorded from the silver dial of the Magne-Gage.

Results and Discussion

Microstructural Analysis

The microstructure of the 9% nickel steel base plate, in the as-received condition, is shown in Fig. 2. The microstructure of this material consists largely of tempered martensite (TM). The TM is a mixture of ferrite (α) and carbide which has precipitated during the tempering heat treatment of as-quenched martensite. Nine percent nickel steel, in the quench-and-tempered condition, also contains approximately 5–10 volume percent of retained austenite (γ). Figure 2B shows the extensive banding present in the as-received material, the lingering result of segregation during the original solidification.

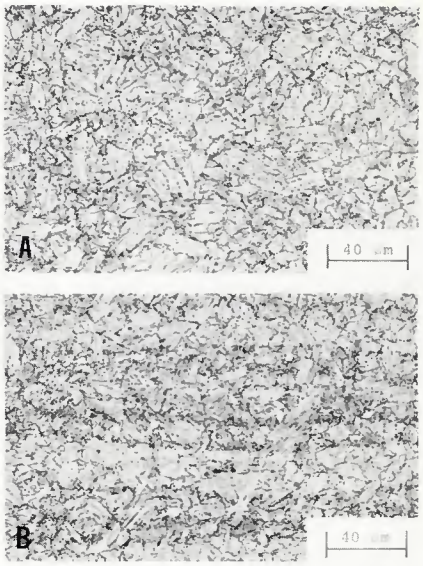

Fig. 2 — Photomicrograph of the material in the as-received condition, Etch A (500X). A — Parallel to the plate surface; B — Perpendicular to the plate surface

In order to verify the heat treatment of the as-received material, a small piece of the plate was austenitized, quenched, and tempered. The steel was austenitized at 816°C (1500°F) for 2 hr, water quenched and tempered at 593°C (1100°F) for 30 min, and air cooled. The as-quenched and quench-and-tempered hardness of this material are listed in Table 4. The microstructure of the mate-

Table 4—Results of Macrohardness and Microhardness Measurements

Heat Treatment	Macro-hardness (HRC)	Micro-hardness (HV, 200-g load)
As-received	20–21	256
As-quenched	36	357
Quench & tempered	20	246
500°C peak temperature thermal cycle	23[a]	255
1000°C peak temperature thermal cycle	37–38[a]	367
1300°C peak temperature thermal cycle	36[a]	353

[a]Calculated values.

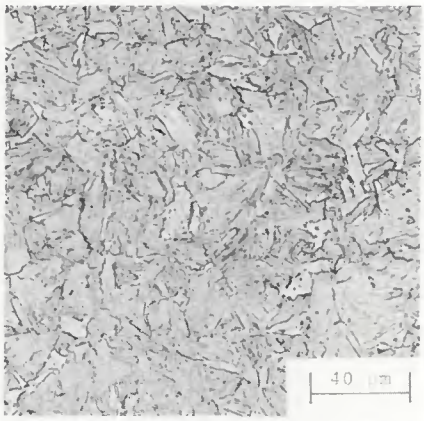

Fig. 3 — Photomicrograph of the material in the as-quenched condition, Etch A (1000X)

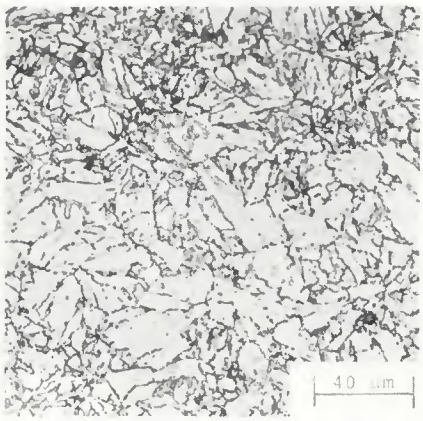

Fig. 4 — Photomicrograph of the material in the quench-and-tempered condition, Etch A (1000X)

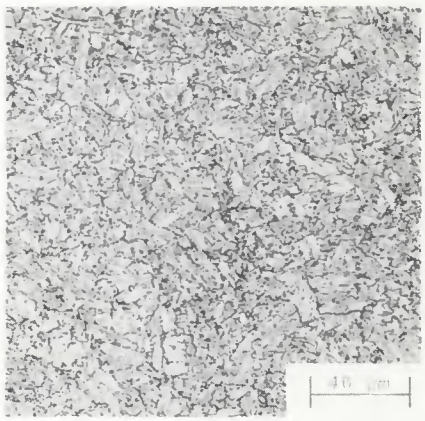

Fig. 5 — Microstructure of material thermally cycled to a peak temperature of 500°C, Etch A (500X)

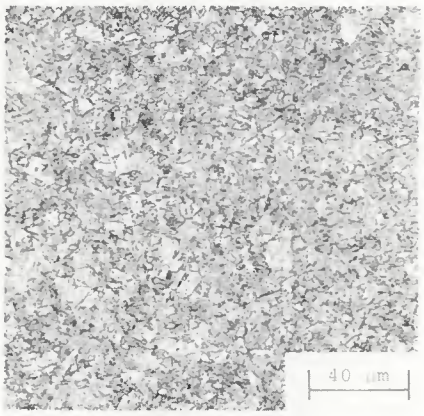

Fig. 6 — Microstructure of material thermally cycled to a peak temperature of 1000°C, Etch A (500X)

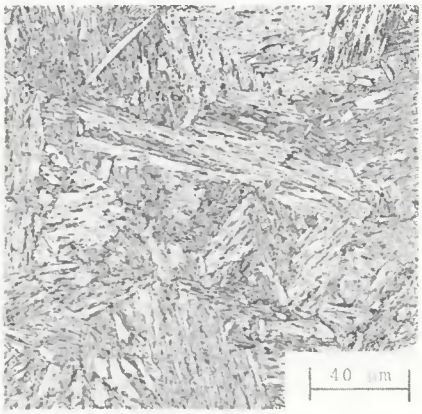

Fig. 7 — Microstructure of material thermally cycled to a peak temperature of 1300°C, Etch A (500X)

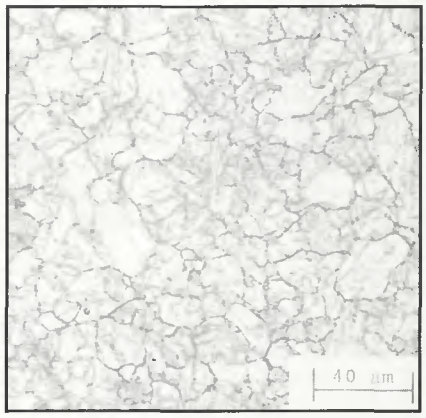

Fig. 8 — Microstructure of material thermally cycled to a peak temperature of 500°C, Etch B (500X)

rial in the as-quenched and quench-and tempered conditions is shown in Figs. 3 and 4, respectively. The microstructure of the as-quenched material consists primarily of martensite (M). The tempering process transforms this martensitic structure into a mixture of ferrite, carbide, and austenite identical to that of the as-received material.

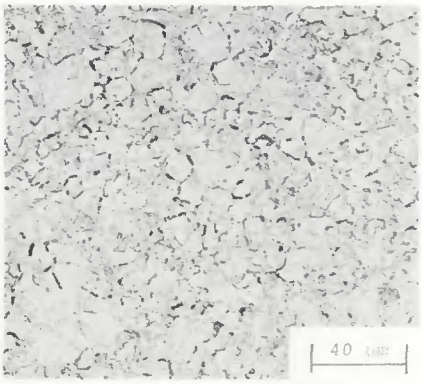

Fig. 9 — Microstructure of material thermally cycled to a peak temperature of 1000°C, Etch B (500X)

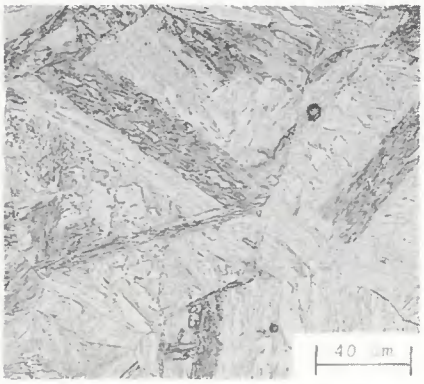

Fig. 10 — Microstructure of material thermally cycled to a peak temperature of 1300°C, Etch B (500X)

Dilatometry was performed during synthetic thermal cycling of specimens. These results indicate the transformation temperatures during the rapid heating and slow cooling portions of the weld thermal cycle. Lower and upper critical temperatures of 618°C (1144°F) and 666°C (1231°F), respectively, were measured for a heating rate of 350°C/s (630°F/s). A martensite start (M_s) temperature of 354°C (669°F) was measured for a cooling rate of 3°C/s (5.4°F/s).

The microstructures of Charpy V-notch specimen blanks thermally cycled to 500°, 1000°, and 1300°C are shown in Figs. 5, 6, and 7, respectively. The same specimens were repolished and etched to reveal the prior-austenite grain size. The microstructural results are shown in Figs. 8, 9, and 10. The results of microhardness testing are given in Table 4. The results of grain size measurements are listed in Table 5.

The microstructure of this material was not noticeably altered by the 500°C peak temperature thermal cycle. Additionally, the microhardness and grain size of the material were unaffected by the low-temperature thermal cycle.

Thermal cycling to a peak temperature of 1000°C had a severe effect on the microstructure of this material. As shown in Fig. 6, the structure was refined by the $\alpha \rightarrow \gamma$ transformation which occurs when heating to a temperature above the upper critical temperature. The $\alpha \rightarrow \gamma$ transformation resulted in a

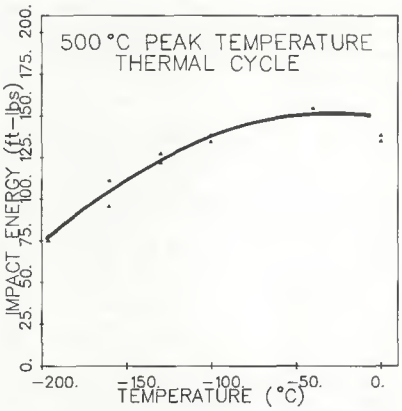

Fig. 11—Impact energy vs. temperature for material thermally cycled to a peak temperature of 500°C

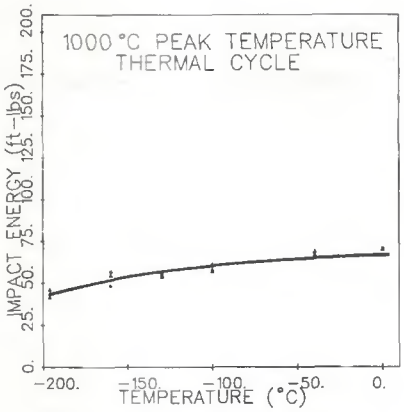

Fig. 12—Impact energy vs. temperature for material thermally cycled to a peak temperature of 1000°C

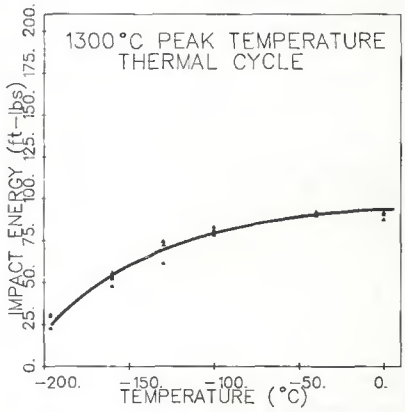

Fig. 13—Impact energy vs. temperature for material thermally cycled to a peak temperature of 1300°C

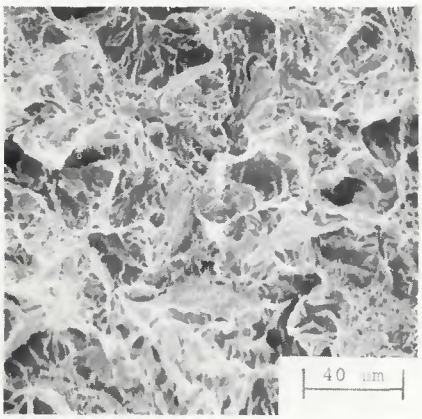

Fig. 14—Fractograph of material thermally cycled to a peak temperature of 500°C and impact tested at −196°C (500X)

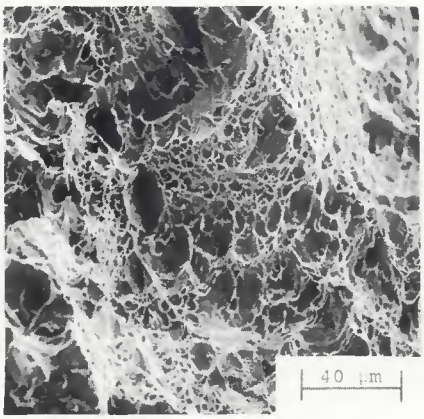

Fig. 15—Fractograph of material thermally cycled to a peak temperature of 1000°C and impact tested at −196°C (500X)

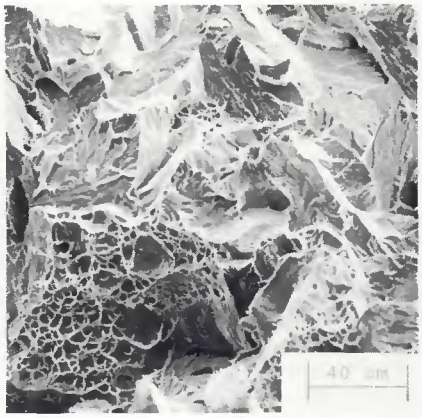

Fig. 16—Fractograph of material thermally cycled to a peak temperature of 1300°C and impact tested at −196°C (500X)

decrease in grain size from ASTM No. 9 in the as-received material to ASTM No. 11. The microhardness of this structure indicates that it was fully hardened. That is, the maximum possible hardness, at this carbon content, had been attained by transformation to 100% martensite. Apparently, the relatively high cooling rate associated with the 1000°C thermal cycle had prevented any significant tempering of martensite during cooling from occurring.

The microstructure of the 9% nickel steel was completely altered by the 1300°C peak temperature thermal cycle. Figure 7 shows the coarse-grained, martensitic structure which results from this thermal treatment. The microhardness of this structure is slightly lower than that of the 1000°C thermally cycled material, but significantly higher than that of the as-received material.

Impact Testing

Impact absorption energy as a function of temperature for material thermally cycled to peak temperatures of 500°C, 1000°C, and 1300°C is shown in Figs. 11, 12, and 13, respectively. The impact absorption energies at −196°C and −162°C, for the base metal and the thermally cycled material, are listed in Table 6. Three specimens were thermally cycled to 1300°C, slowly cooled to room temperature, and quenched to −196°C, prior to impact testing at 0°C. The results of these tests are also listed in Table 6.

Fractography

Fractographs of Charpy V-notch specimens of the three thermal cycles, impact tested at −196°C, are shown in Figs. 14, 15, and 16. Fractographs of similar specimens thermally cycled to 1000° and 1300°C, and impact tested at 0°C, are shown in Figs. 17 and 18. The material thermally cycled to a peak temperature of 500°C had an impact absorption energy of 104 J (77 ft-lb) at −196°C. The Charpy V-notch fracture surface, shown in Fig. 14, indicates that failure occurred by a mixed mode of microvoid coalescence and ductile tearing. This failure mode is characteristic of high-strength, high-toughness materials (Ref. 23).

The material thermally cycled to a peak temperature of 1000°C had impact absorption energies of 59 J (44 ft-lb) at −196°C and 93 J (68.5 ft-lb) at 0°C. Examination of the fracture surface of the Charpy specimen tested at −196°C indicates that failure occurred by a mixed mode of microvoid coalescence and ductile tearing. Additionally, some secondary cracking occurred normal to the fracture surface. A secondary crack is present in the center of the fractograph in Fig. 15. Examination of the fracture surface of the

Table 5—Results of Grain Size Measurements

Heat Treatment	ASTM Grain Size
As-received	9
500°C peak temperature thermal cycle	9
1000°C peak temperature thermal cycle	11–12
1300°C peak temperature thermal cycle	4–5

Table 6—Impact Absorption Energies of Thermally Cycled 9% Nickel Steel

Heat Treatment	Impact Absorption Energy J (ft-lb) −196°C	Impact Absorption Energy J (ft-lb) −162°C	Upper Shelf Energy J (ft-lb)
As-received	112 (82)	133 (98)	245 (181)
500°C peak temperature thermal cycle	104 (77)	140 (103)	185 (136)
1000°C peak temperature thermal cycle	59 (44)	72 (53)	93 (69)
1300°C peak temperature thermal cycle	38 (28)	71 (52)	123 (91)
1300°C peak temperature thermal cycle, quenched to −196°C prior to testing	–	–	133 (98)

Table 7—Results of Retained Austenite Measurements by X-Ray Diffraction and Magne-Gage

Heat Treatment	X-Ray Diffraction (v-% Retained γ)	Magne-Gage (Silver Dial Reading)
As-received	9.4 ± 0.3	32.8 ± 0.7
500°C peak temperature thermal cycle	3.9 ± 0.6	29.5 ± 0.7
1000°C peak temperature thermal cycle	<1.0	24.2 ± 0.3
1300°C peak temperature thermal cycle	2.9 ± 0.1	29.7 ± 1.7

specimen tested at 0°C showed an increase in the dimpled area characteristic of a microvoid coalescence-type failure.

The material thermally cycled to a peak temperature of 1300°C had impact absorption energies of 38 J (28 ft-lb) at −196°C and 123 J (90.5 ft-lb) at 0°C. Examination of the fracture surface of the specimen tested at −196°C indicated that failure had occurred by a mixed mode of transgranular quasi-cleavage and microvoid coalescence. Dimpled areas indicating a ductile mode of failure were extremely localized. A significant amount of secondary cracking occurred in areas of quasi-cleavage. A similar specimen, impact tested at 0°C, failed by a mechanism of microvoid coalescence. The fracture surface of this specimen, shown in Fig. 18, contained the extensive dimpling associated with this type of failure.

Retained Austenite

Results of the x-ray diffraction measurements for retained austenite are given in Table 7. The 9% nickel steel plate used in this investigation was found to have approximately 9.4 v-% retained austenite in the as-received condition. The retained austenite contents of material thermally cycled to peak temperatures of 500° and 1300°C were found to be approximately 4 and 3 v-%, respectively. With the x-ray diffraction technique used in this investigation, no retained austenite was detected in the material thermally cycled to a peak temperature of 1000°C. The lower limit of detection for this technique was estimated to be approximately 1 v-%. Therefore, the material thermally cycled to a peak temperature of 1000°C probably contains some finite amount of retained austenite less than 1 v-%.

Results of the Magne-Gage measurements for estimating retained austenite content are listed in Table 7. These results are in good agreement with the results from x-ray diffraction measurements. The correlation between the Magne-Gage and x-ray diffraction measurements was evaluated using the Pearson correlation coefficient (Ref. 24). This coefficient, which is used to measure the strength of the linear relationship between two variables, was found to be 0.9. Although further research is needed in this area, these results indicate that the Magne-Gage has potential as an inexpensive and qualitative method for estimating the retained austenite content of this material.

Autogenous welds were made on 9% nickel steel plate using the GTAW process and an energy input of 45 kJ/in. The microstructure of the weld in the coarse-grained region of the HAZ is shown in Fig. 19. The microstructure compares favorably with the synthetically produced coarse-grained HAZ, shown in Fig. 7. The results of a microhardness traverse across the true weld HAZ are shown in Fig. 20.

Microhardness data measured in the true weld heat-affected zone were correlated with similar data from synthetic weld heat-affected zones. Using the F(s,d) calculations discussed previously, it was found that synthetic thermal cycles to peak temperatures of 1300° and 1000°C correspond to distances of 0.25 mm (0.01 in.) and 0.75 mm (0.03 in.), respectively, from the fusion line in the actual weld. The microhardness of the true weld HAZ, at a distance of 0.20 mm

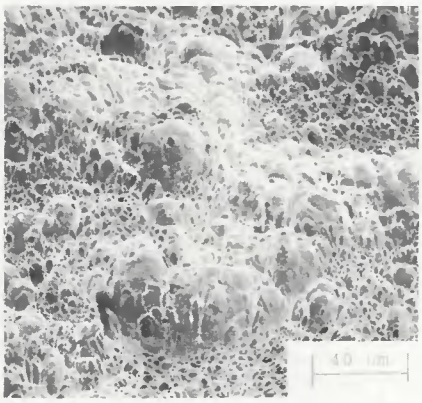

Fig. 17—Fractograph of material thermally cycled to a peak temperature of 1000°C and impact tested at 0°C (500X)

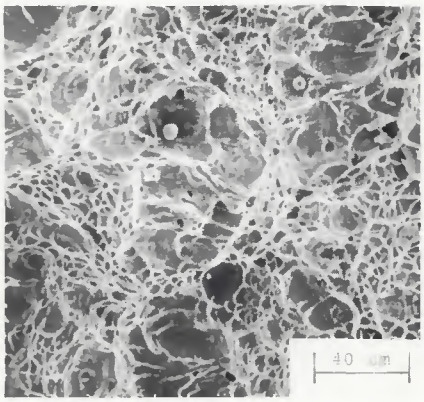

Fig. 18—Fractograph of material thermally cycled to a peak temperature of 1300°C and impact tested at 0°C (500X)

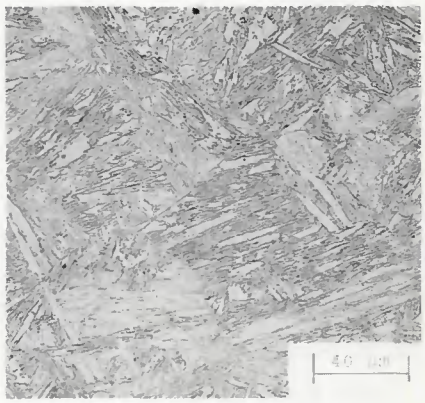

Fig. 19—Microstructure of the coarse-grained region of the true HAZ in a 9% nickel steel weld, Etch A (500X)

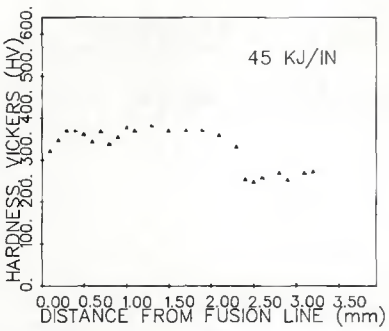

Fig. 20—Microhardness traverse of the true weld HAZ in an autogenous, GTA weld on 9% nickel steel

(0.008 in.) from the fusion line, was HV 347. This correlates well with the value of HV 353 obtained for material synthetically thermal cycled to 1300°C. The microhardness of the true weld HAZ, at a distance of 0.70 mm (0.028 in.) from the fusion line, was HV 367. This is identical to the value obtained for material thermally cycled to a peak temperature of 1000°C. The maximum microhardness measured in the true weld HAZ, HV 381, occurred at a distance of 1.3 mm (0.05 in.) from the fusion line.

Conclusions

The effect of weld thermal cycles on the impact absorption energy of the weld HAZ of 9% nickel steel at cryogenic temperatures was evaluated. The primary findings of this investigation were:

1. The impact absorption energy of the weld HAZ of 9% nickel steel does not decrease below the limit of 34 J at −196°C (25 ft-lb at −320°F) as specified in ASTM 553-I.

2. The upper shelf of the impact energy curve was lowest for the material thermally cycled to a peak temperature of 1000°C (1832°F).

3. The impact absorption energy, measured at −196°C, was lowest for the material thermally cycled to a peak temperature of 1300°C (2372°F). This reduction in impact absorption energy was probably the result of the grain coarsening which normally occurs in this region of the weld HAZ.

4. Material thermally cycled to peak temperatures of 500° and 1000°C (932° and 1832°F) and impact tested at −196°C failed by a mixed mode of microvoid coalescence and ductile tearing. Material thermally cycled to a peak temperature of 1300°C and impact tested at −196°C failed by a mixed mode of transgranular quasi-cleavage and microvoid coalescence.

5. The retained austenite content of this steel, as measured by x-ray diffraction, is approximately 9 v-% in the as-received condition.

6. Synthetic thermal cycling of this material to peak temperatures of 500° and 1300°C significantly decreases the retained austenite content. Synthetic thermal cycling to a peak temperature of 1000°C reduces the retained austenite content to an undetectible level.

7. The decreased impact toughness of this material, after synthetic thermal cycling, is apparently partly caused by local reductions in the retained austenite content. The reduction in retained austenite content results in a decrease in the upper shelf of the impact energy vs. temperature curve for all three thermal cycles.

8. The Magne-Gage, although normally used to measure small amounts of ferrite in a non-magnetic matrix, can be used to measure, qualitatively, small amounts of austenite in a ferritic matrix. The Magne-Gage measurements of retained austenite content were in good agreement with x-ray diffraction measurements for the material and heat treatments used in this investigation.

9. Procedures utilized previously for constructing and producing weld thermal cycles in low-alloy steels can be effectively used for 9% nickel steel. The synthetic weld heat-affected zones produced in this investigation correlate well with actual weld heat-affected zones in this material.

References

1. Pense, A. W., and Stout, R. D. May 1975. Fracture toughness and related characteristics of the cryogenic nickel steels. WRC Bulletin No. 205.

2. Wilson, A. D. May 1981. Variables influencing the toughness of 9% nickel steel. American Gas Association Transmission Conference, Atlanta, Georgia.

3. Strife, J. R., and Passoja, D. E. 1980. The effect of heat treatment on microstructure and cryogenic fracture properties of 5 Ni and 9 Ni steel. *Met. Trans.* 11A(8): 1341–1350.

4. Marschall, C. W., Hehemann, R. F., and Troiano, A. R. 1962. The characteristics of 9% nickel low carbon steel. *Trans. ASM* 55: 135–148.

5. Syn, C. K., Jin, S., and Morris, J. W., Jr. 1976. Cryogenic fracture toughness of 9 Ni steel enhanced through grain refinement. *Met. Trans.* 7A(12): 1827–1832.

6. Kim, K. J., and Schwartz, L. H. 1978. On the effects of intercritical tempering on the impact energy of Fe-9Ni-0.1C. *Materials Science and Engineering* 33: 5–20.

7. Schwartz, L. H. July 1976. Final report to AISI on Project 66-32. Dept. of Mat. Sci. and Eng., Northwestern University, Evanstown, Ill.

8. Kim, J. I., Kim, H. Jae, and Morris, J. W., Jr. 1984. The role of constituent phases in determining the low temperature toughness of 5.5 Ni cryogenic steel. *Met. Trans.* 15A(12): 2213–2219.

9. Nippes, E. F. 1959. The weld heat-affected zone. *Welding Journal* 38(1): 1-s to 18-s.

10. Nippes, E. F., and Savage, W. F. 1949. Development of specimen simulating weld heat-affected zones. *Welding Journal* 8(11): 534-s to 546-s.

11. Nippes, E. F., and Sibley, C. R. 1956. Impact performance of synthetically reproduced heat-affected zone microstructures in T-1 steel. *Welding Journal* 35(10): 473-s to 480-s.

12. Toughness of 9% Nickel Steels. Osaka Gas Co., Ltd., Ishikawajima-Harima Heavy Industries Co., Ltd., and Sumitomo Metal Industries, Ltd., June 26–27, 1980.

13. Bruscato, R. M. 1981. The measurement of crack arrest fracture toughness in welded 9% nickel steels used in cryogenic storage tanks. *Welding Journal* 60(7): 112-s to 120-s.

14. Fracture Characteristics of Nine Percent Nickel Steel Plate and Its Welded Joint. Nippon Steel Corporation, June 1980.

15. Bruner, J. P., and Sarno, D. A. 1978. Steels for cryogenic service. *Advances in Cryogenic Engineering* 24: 529–539.

16. Dhooge, A., Provost, W., and Vinckier, A. July 1982. Weldability and fracture toughness of quench and tempered 9% nickel steel, part I—weld simulation testing, part II—wide plate testing. *WRC Bulletin No. 279.*

17. Toyosada, M. 1979. Mechanical properties and fracture toughness of 9% nickel steel and its welded joint on LNG carrier. *Hitachi Zosen Tech. Rev.* 40(2): 38–49.

18. Stout, R. D., and Pense, A. W. May 1981. Crack arrest properties of 9% nickel cryogenic steels. Final Report, GRI 80/0037.

19. Ripling, E. J. 1982. Unpublished work.

20. Nippes, E. F., Merrill, L. L., and Savage, W. F. 1949. Cooling rates in arc welds in ½-in. plate. *Welding Journal* 28(11): 556-s to 564-s.

21. Miller, R. L. 1964. A rapid x-ray method for the determination of retained austenite. *Trans. ASM* 57: 892–899.

22. Kotecki, D. J. 1982. Extension of the WRC ferrite number system. *Welding Journal* 61(11): 352-s to 361-s.

23. Fractography and Atlas of Fractographs. 1974. *ASM Metals Handbook,* Vol. 9, 8th Edition, American Society for Metals, Metals Park, Ohio.

24. Neter, J. and Wasserman, W. 1974. *Applied Linear Statistical Models,* Richard D. Irwin, Inc., Homewood, Ill.